Supporting Information

Boosting High-Performance in Lithium-Sulfur Batteries via Dilute Electrolyte

Feixiang Wu,*,† Fulu Chu,† Guillermo A. Ferrero,‡ Marta Sevilla,‡ Antonio B. Fuertes,‡ Oleg Borodin,⊥ Yan Yu,*,§,ξ,⊤ and Gleb Yushin*,∇

† School of Metallurgy and Environment, Engineering Research Center of the Ministry of Education for Advanced Battery Materials, Central South University, Changsha 410083 P. R. China.

‡ Instituto Nacional del Carbón (CSIC), Fco. Pintado Fe 26, Oviedo 33011, Spain

⊥ Energy Storage Branch, Sensors and Electron Devices Directorate, US Army Research Laboratory, Adelphi, MD 20783, USA

§ Hefei National Laboratory for Physical Sciences at the Microscale Department of Materials Science and Engineering, Key Laboratory of Materials for Energy Conversion, Chinese Academy of Sciences (CAS), University of Science and Technology of China, Hefei, Anhui 230026, P. R. China

ξ Dalian National Laboratory for Clean Energy (DNL), Chinese Academy of Sciences (CAS), Dalian 116023, P. R. China

⊤ State Key Laboratory of Fire Science, University of Science and Technology of China, Hefei, Anhui 230026, P. R. China

∇ School of Materials Science and Engineering, Georgia Institute of Technology, Atlanta, GA 30332, USA.

AUTHOR INFORMATION

* Corresponding Authors

Email: feixiang.wu@csu.edu.cn
Email: yanyumse@ustc.edu.cn
Email: yushin@gatech.edu

EXPERIMENTAL SECTION

Synthesis of porous carbon capsule (CC). The N-doped carbon capsules were fabricated following our previous procedure. [1] Firstly, silica particles with a hollow core and a mesoporous shell were synthesized as reported by Unger et al. [2] Secondly, the silica particles were impregnated via dropwise impregnation technique with a 2 M $FeCl_3$ solution in ethanol (around 0.27 g $FeCl_3$/g silica). Afterwards, the impregnated sample was exposed to pyrrole (Aldrich, 99%) vapors at 25 ºC for 22 h in closed vessel. The dark solid thus obtained was heat-treated at 850 ºC (3ºC/min) for 1 h under N_2. Finally, the carbonized composite was treated with hydrofluoric acid for 4 days to dissolve the silica framework. The carbon residue was recovered by filtration, washed with abundant distilled water and dried in an oven at 120 ºC for several hours.

Preparation of CC-S composite. CC-S composites were prepared by thoroughly milling massive sulfur (Sigma-Aldrich, >99.5%, USA) and porous carbon, followed by melt-infiltration of the sulfur on a hot-plate at 150 °C for 12 hours in air. Then the access sulfur was evaporated at 180 °C. During sulfur evaporation, the mass change was monitored. The sulfur contents in CC-S was 71 wt%, based on TG measurement and the mass change of the sample before and after sulfur infiltration.

Material characterization. Powder X-ray diffraction (Rigaku D/max-2550V) using Cu-Kα radiation was employed to identify the crystalline phase of the nanocomposite. SEM micrographs have been collected on a field-emission LEO microscope (Zeiss, Germany) at a working distance of 3-6 mm and an accelerating voltage of 2-3 kV. A transfer tool between the SEM working

chamber and a glovebox was used for inserting the samples (cycled electrodes) in order to avoid their exposure to air during transfer. High-angle annular dark-field (HAADF)-STEM imaging combined with (energy-dispersive X-ray) EDX measurements were carried out at 60 kV with an advanced TEM (JEOL ARM200F, JEOL Co. Ltd.), equipped with a cold field-emission gun and a CETCOR image corrector (CEOS Co. Ltd.). EDX spectra and elemental maps were obtained by using a 50 mm^2 Bruker EDX detector. N_2 physisorption experiments were carried out at -196 °C on a Quadrasorb apparatus (40-60 mg sample) from Quantachrome Instruments. Prior to all measurements, the samples were outgassed at vacuum for 24 h under vacuum. The ionic conductivities of different electrolytes were measured by a conductivity meter (Leici, DDSJ-319L, China) at room temperature (24~25 °C).

Electrochemical Measurements. For cathode preparation, the CC-S composite powder was mixed with carbon black (Alfa Aesar, carbon black, super P, metals basis, >99%) and polyvinylidene fluoride (PVDF) binder at the weight ratio of 80:10:10 in an N-methyl-2-pyrrolidone (NMP) to form a homogeneous slurry. Then, the slurry was cast on an aluminum foil through the doctor-blade technique, followed by drying at 50 °C for 12 h under vacuum. The mass loading of active material (sulfur) was controlled to be 2.0, 3.8 and 5.2 mg cm^{-2}. Subsequently, circular samples with a diameter of 10 mm were punched out for electrochemical tests in CR2032 coin cells. Coin cells were assembled with a 0.1 M or 1M or 2M or 3M, or 5M lithium bis(trifluoromethanesulfonyl)imide salt solution in distilled dimethoxyethane:1,3-dioxolane (1:1, v:v) with 1 wt.% (based on mass of solvents) of $LiNO_3$ (Alfa Aesar, anhydrous, 99.99%, USA) additive as electrolyte (the volume of salt was ignored). Celgard 2400 (Celgard, USA) was used as a separator and pure Li foil anode as a counter electrode in half-cells. The volume of electrolyte injected in coin cells is set to about 15 μL per 1 mg of sulfur. The cells were equilibrated for 24 h before operation. The coin cells assembled inside an Ar glovebox (< 0.2 ppm of H_2O, < 0.6 ppm of O_2, Mbraun, Germany) were charged and discharged over a voltage range of 1.6-2.8 V versus Li/Li^+ for the electrochemical test at room temperature by using an Arbin battery test system (Arbin Instruments, USA) and the Neware system (Shenzhen, China). The cells were activated at small C rates and then the cycle

durability test was continued at C/2. The specific capacities were calculated based on the mass of sulfur.

Simulations Methodology. Molecular dynamics (MD) simulations were performed on the DME:DIOX-LiTFSI electrolytes doped with ~0.4M-0.5M of Li_2S_2 or Li_2S_4 using polarizable APPLE&P force field[3, 4] in order to obtain further insight into the polysulfide aggregation low (0.1M), intermediate (1M) and high (3M) LiTFSI concentrations. A previously developed and validated many-body polarizable force field APPLE&P was used for the LiTFSI-H_2O interactions[5] and polysulfides.[4] Functional form of APPLE&P force field is described elsewhere.[3] MD simulation code and manual are given in SI to ref.[6]. An additional validation of the force field was performed by comparison of the predicted self-diffusion coefficients for 1M, 3M DME:DIOX-LiTFSI and for 0.25M Li_2S_4 with experimental values as shown in Fig. S11. An excellent agreement between the predicted and measured values indicates that the interaction between solvent and salts are accurately captured in the model. Similar Li^+ and solvent self-diffusion coefficients for 0.25M Li_2S_4 indicates lack of Li_2S_4 aggregation as it would significantly decrease Li^+ self-diffusion coefficient.

The DME:1.49DIOX solvent mixtures were mixed with Li_2S_2 or Li_2S_4 at 0M, 0.1M, 1.0M and 3.0M LiTFSI salt concentrations. An MD simulation cell had linear dimensions from 51 Å to 56 Å. The initial configuration for simulations was created in the gas-phase with the linear box dimention of ~100 Å. The system linear dimensions were scaled to 58 Å during 2 ns MD simulation run at 500 K with an extra repulsion added between sulfides, yielding an even distribution of sulfides throughout the MD simulation cell. First MD simulations were performed at 363 for 50-100 ns with the first half of trajectory discarded as equilibration. After than temperature was decreased to 298 K and additional 54-192 ns simulations were performed with the exception of 0.5M Li_2S_2 in 3M LiTFSI that were simulated only at 363 K due to sluggish dynamics. The length of MD simulation runs is given in Table S1. The Ewald summation method was used for the electrostatic interactions between permanent charges with permanent charges and permanent charges with induced dipole moments with $k = 6^3$ vectors. Multiple timestep integration was employed with an inner

timestep of 0.5 fs (bonded interactions); a central time step of 1.5 fs for all nonbonded interactions within a truncation distance of 7.0-8.0 Å and an outer timestep of 3.0 fs for all nonbonded interactions between 7.0 Å and the nonbonded truncation distance of the smaller of 14 Å. The reciprocal part of Ewald was updated only at the largest of the multiple time steps. A Nose-Hoover thermostat and a barostat were used to control the temperature and pressure with the associated frequencies of 10^{-2} and 0.1 x 10^{-4} fs. The atomic coordinates were saved every 2 ps for post-analysis. Finite Size Correction (FSC) correction, self-diffusion coefficients and conductivity were extracted following previously described methodologies.[3]

Results and Discussion

No shells or additional protection on CCs was used in order to maximize the sensitivity of cell performance to electrolyte compositions. The CCs are hollow spheres with a core diameter of 300±40 nm and a microporous carbon shell of ~50 nm in thickness (Fig. S1a-b). The S was infiltrated into the carbon mesopores and large central void in CC by melt infiltration at 150 °C, forming a homogeneous CC-S composite (Fig. S1c-d) with S content of ~71 wt.%, as determined by the weight increase and thermogravimetric analysis (TGA) studies (Fig. S2). The Brunauer-Emmett-Teller specific surface area (BET SSA) measurements of CC and CC-S demonstrate large reduction of BET SSA after S infiltration (Fig. S3), which further proves the successful S confinement in the porous CC. No significant changes in the morphology of CC was observed after S infiltration so that the CC-S surface remained smooth without S particles on the external surface (Fig. S1c and d). The homogeneous distribution of S in CC-S was confirmed by energy-dispersive X-ray (EDX) mapping (Fig. S1d). X-ray diffraction (XRD) analyses showed an amorphous carbon phase and the absence of any crystalline S phases, indicating uniform confinement of S within the carbon nano-pores (Fig. S4).

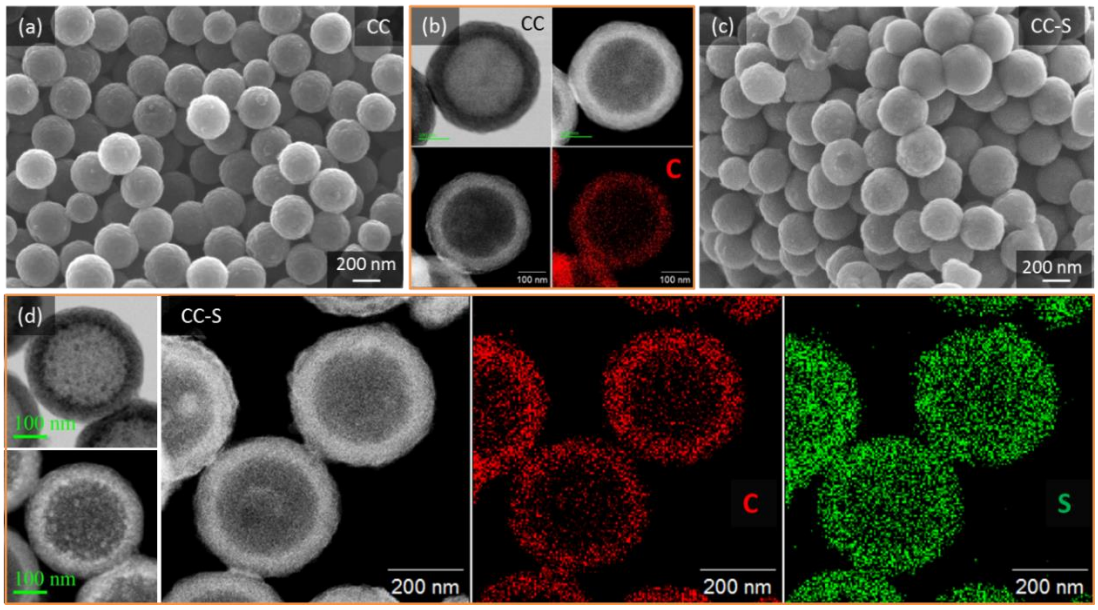

Figure S1. Morphology characterization of the synthesized CC and CC-S composites: SEM images of (a) empty CC, and (c) CC-S; TEM images and the corresponding EDX mapping of (b) CC, and (d) CC-S, displaying a uniform S infiltration in porous CC.

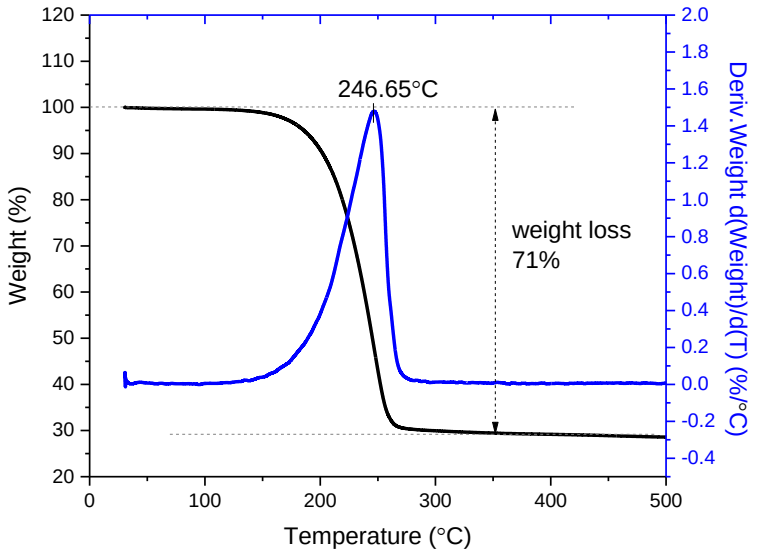

Figure S2. TG curve of CC-S composite.

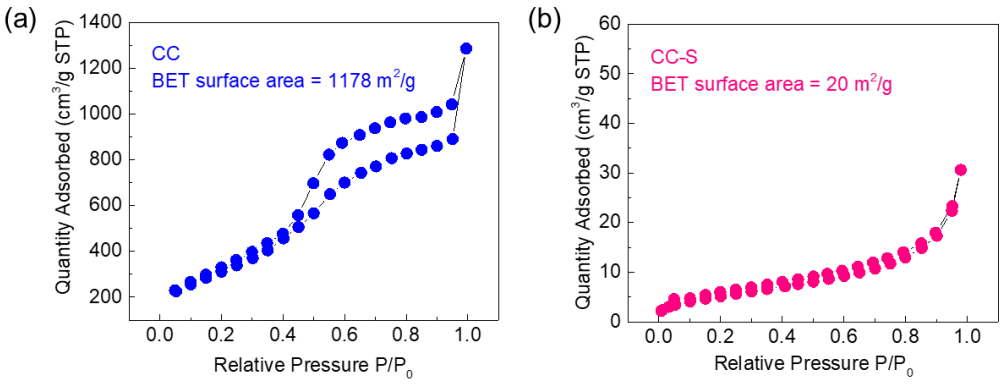

Figure S3. BET surface area of CC and CC-S composite.

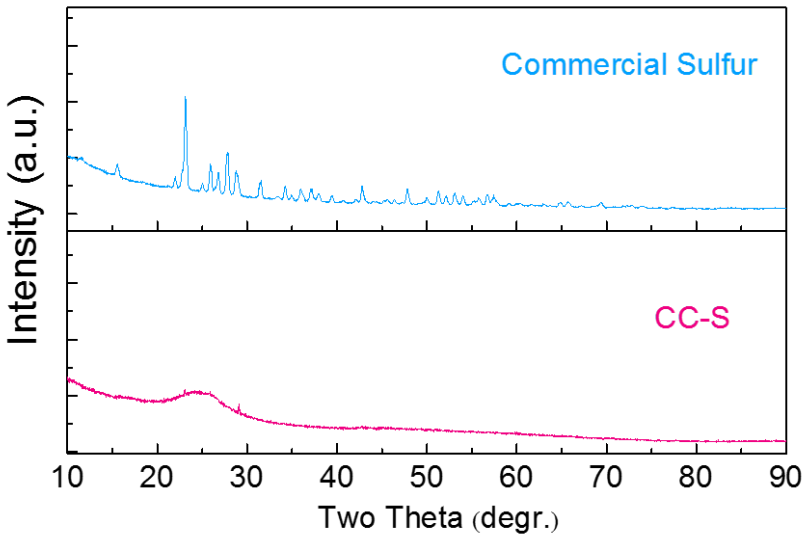

Figure S4. XRD pattern of CC-S composite.

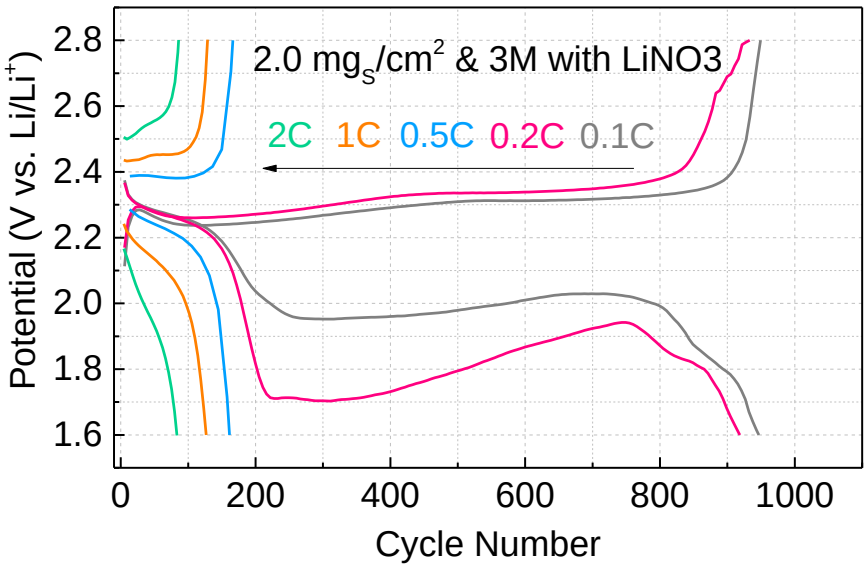

Figure S5. Discharge-charge profiles at different C rates in 3M electrolyte.

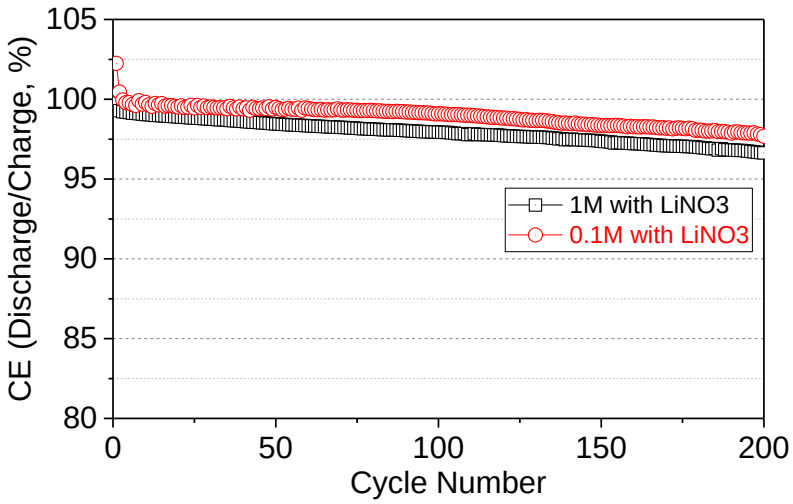

Figure S6. Coulombic efficiency (CE) of the cells in 0.1M and 1M electrolytes.

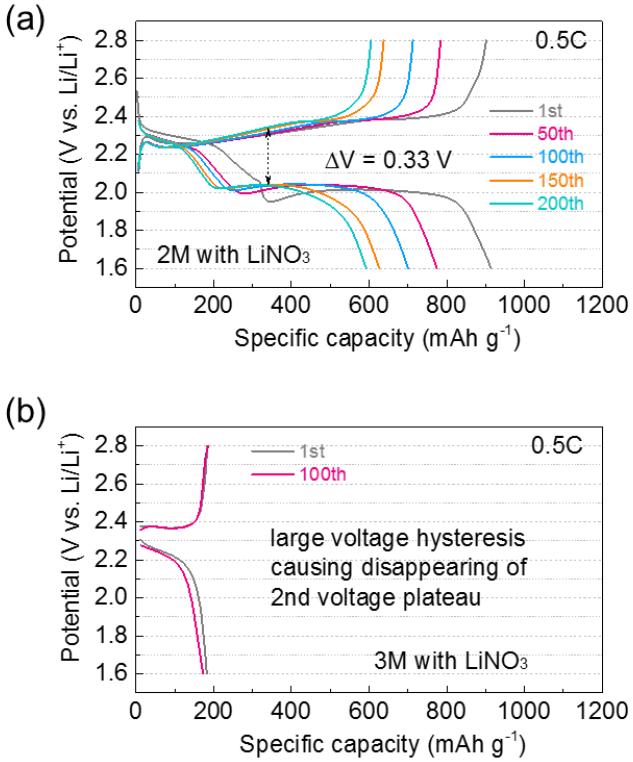

Figure S7. Changes in discharge-charge profiles at 0.5 C rate in (a) 2M and (b) 3M electrolyte.

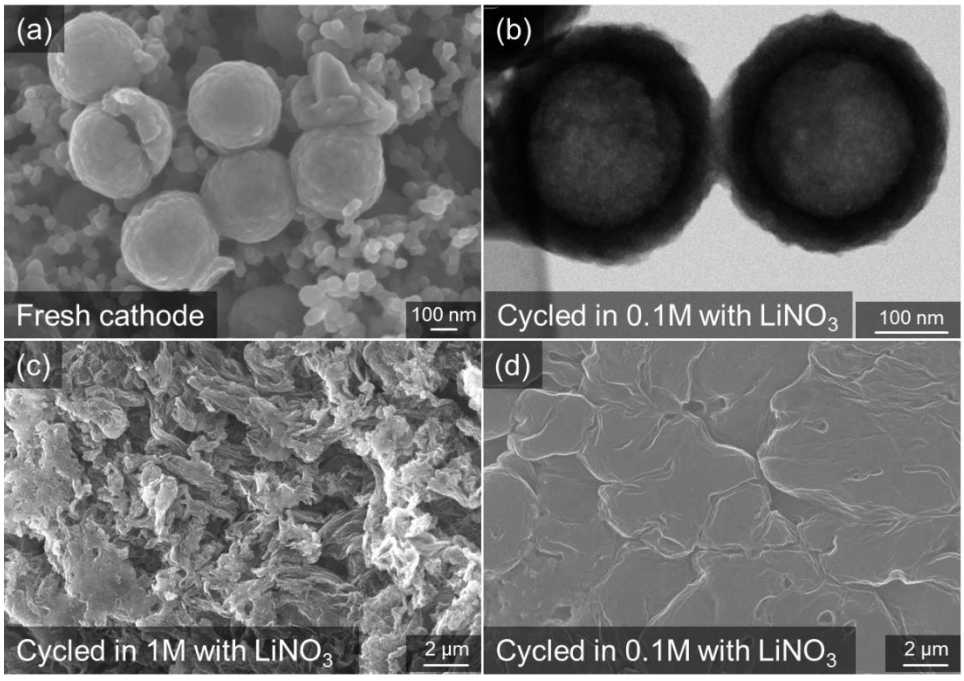

Figure S8. (a) SEM image of fresh cathode, (b) TEM image of cycled CC-S composite particle in 0.1M electrolyte after 200 cycles, and SEM images of cycled Li anode in (c) 1M and (d) 0.1M electrolytes.

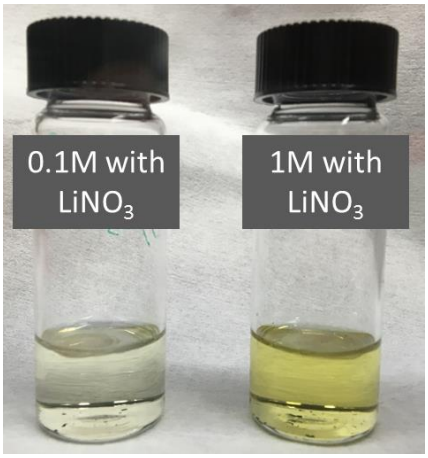

Figure S9. Color change of cycled electrolytes (with cycled separator inside)(200 cycles): (a) 0.1M and (b) 1M.

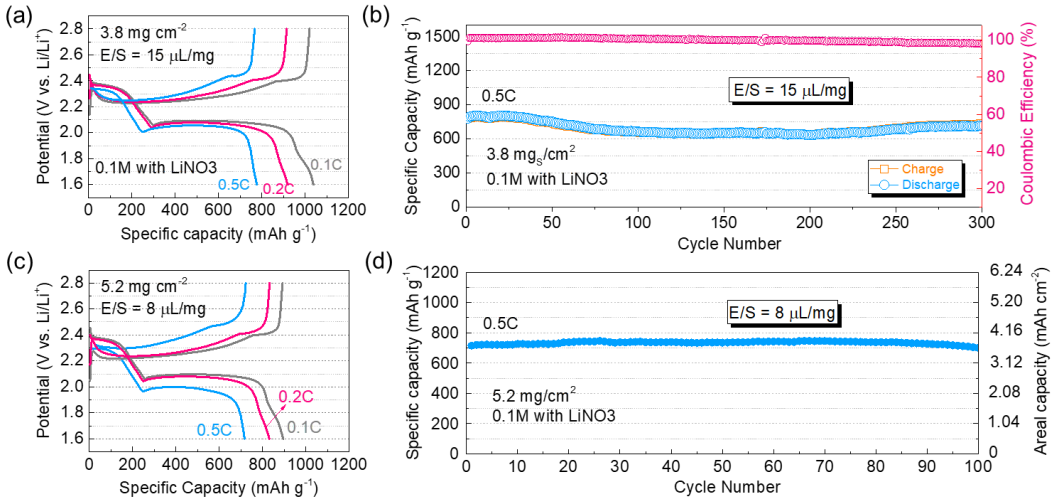

Figure S10. Electrochemical characterizations of high mass loading CC-S cathodes in ultra-dilute (0.1M) electrolyte with E/S ratio: voltage profiles at different C rates under different S mass loadings and E/S ratios (a: 3.8 mg·cm^{-2}, 15 μL·mg^{-1}; c: 5.2 mg·cm^{-2}, 8 μL·mg^{-1}); cycle stability at 0.5C under different S mass loadings and E/S ratios (b: 3.8 mg·cm^{-2}, 15 μL·mg^{-1}; d: 5.2 mg·cm^{-2}, 8μL μL·mg^{-1}), displaying the ability of the ultra-dilute electrolyte to simultaneously handle high S loading and low E/S ratio.

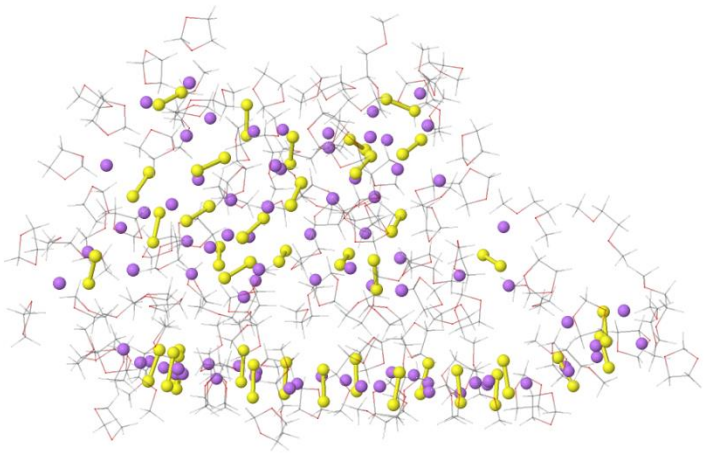

Figure S11. The Li_2S_2 aggregate formed in dilute 0.1M LiTFSI with 0.5M Li_2S_2 electrolyte at the end of MD simulations.

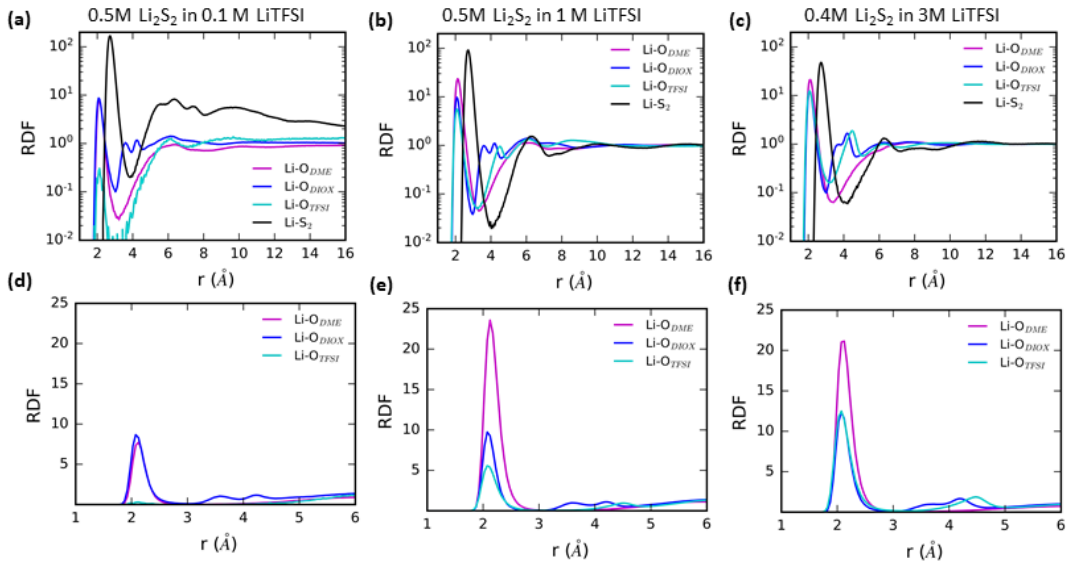

Figure S12. The intermolecular radial distribution functions (RDFs) for Li-O_{DME}, Li-O_{DIOX}, Li-O_{TFSI} and Li-$S_{(S2)}$ from MD simulations of Li_2S_2 in DME:DIOX-LiTFSI.

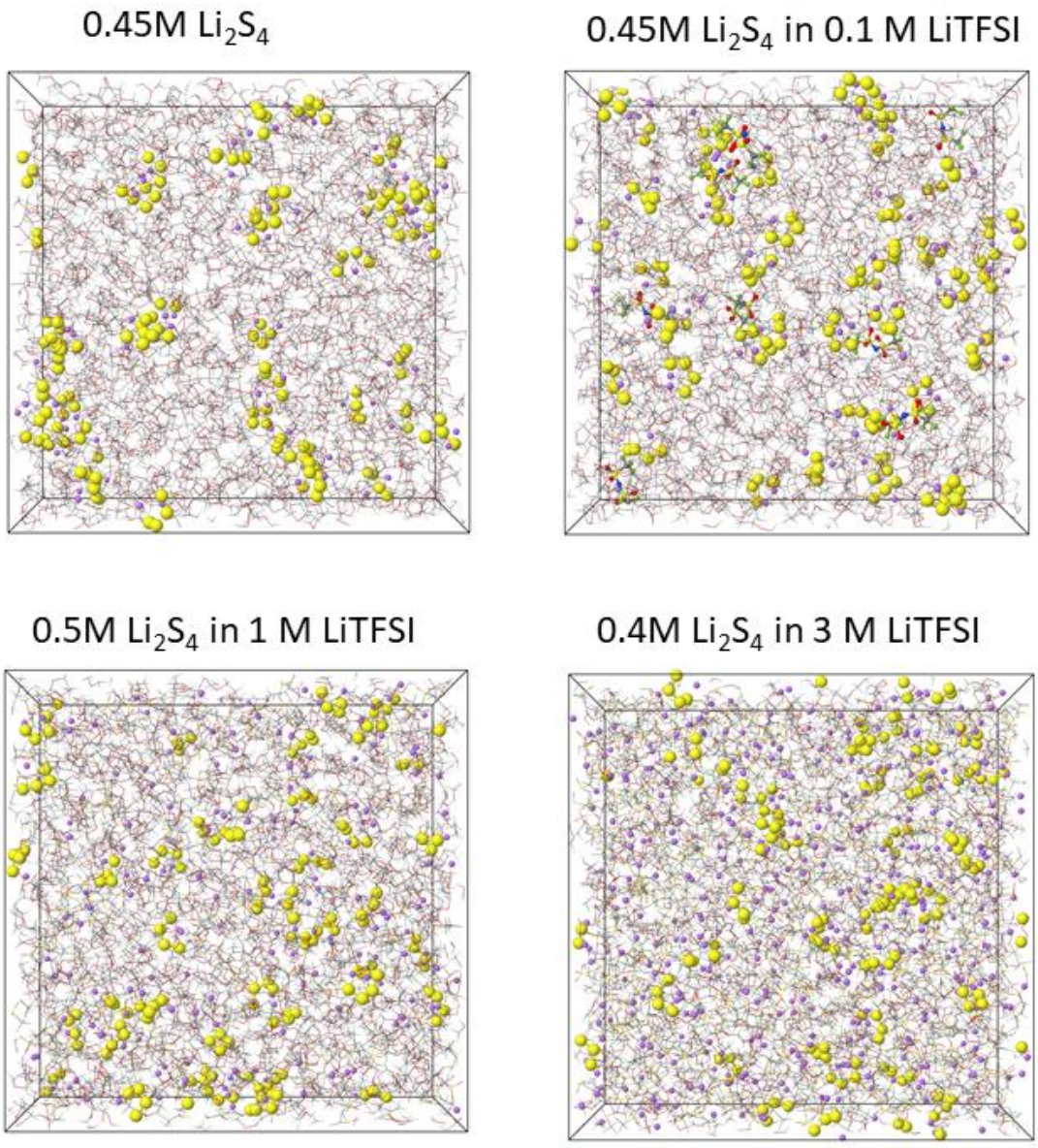

Figure S13. Snapshots of MD simulations boxes highlighting S_4 anions (shown in yellow), solvent and $TFSI^-$ are shown as a wire frame from MD simulations.

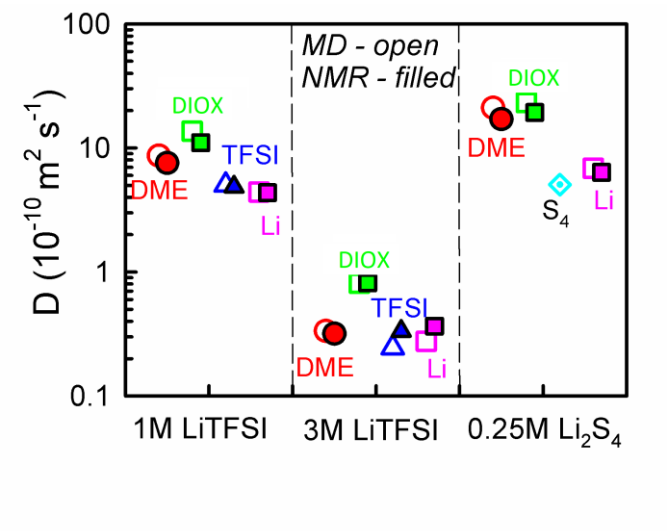

Figure S14. Self-diffusion coefficients from MD simulations at 298 K using APPLE&P force field and previously reported NMR measurements.[7]

Table S1. The composition of MD simulation cells and simulation time at 298 K.

molecules	composition	composition	composition	composition	composition
DME	384	384	384	384	300
DIOX	572	572	572	572	446
LiTFSI	96	336	8	96	336
Li_2S_2			40	42	42
Nominal concentration	1M LiTFSI	3M LiTFSI	0.5M Li_2S_2 0.1M LiTFSI	0.5M Li_2S_2 1M LiTFSI	0.4M Li_2S_2 3M LiTFSI
Exact concentration	1.03M LiTFSI	3.06M LiTFSI	0.48M Li_2S_2 0.10M LiTFSI	0.44M Li_2S_2 1.02M LiTFSI	0.36M Li_2S_2 2.88M LiTFSI
Simulation time (ns)	82	187.5	91.6	192.7	90.4
DME	384	384	384	384	300
DIOX	572	572	572	572	446
LiTFSI	0	0	10	96	336
Li_2S_4	20	40	40	42	42
Nominal concentration	0.25M Li_2S_4	0.5M Li_2S_4	0.5M Li_2S_4 0.1M LiTFSI	0.5M Li_2S_4 1M LiTFSI	0.4M Li_2S_4 3M LiTFSI
Exact concentration	0.24M Li_2S_4	0.48M Li_2S_4	0.48M Li_2S_4 0.12M LiTFSI	0.44M Li_2S_4 1.02M LiTFSI	0.37M Li_2S_4 2.97M LiTFSI
Simulation time (ns)	60	204	89.4	98.2	89.4

molecules	composition	composition	composition
DME	384	384	384
DIOX	572	572	572
LiTFSI	8	8	8
			20 Li_2S_2 20 Li_2S_4
Exact concentration	0.10M LiTFSI	0.10M LiTFSI	0.24M Li2S2 + 0.24M Li_2S_4 + 0.1M LiTFSI
Simulation time (ns)	80.2	71.4	26

Table S2. Transport properties of DME:DIOX – LiTFSI electrolytes from MD simulations at 298 K as a function of salt concentration.

Property \ salt concentration	0.1 M (replica 1)	0.1M (replica 2)	1.03M	3.06M
D(DME) (10^{-10} m^2 s^{-1})	22.5	25.8	8.0	0.31
D(DIOX) (10^{-10} m^2 s^{-1})	25.9	26.6	12.7	0.78
D($TFSI^-$) (10^{-10} m^2 s^{-1})	10.0	9.4	4.5	0.24
D(Li^+) (10^{-10} m^2 s^{-1})	8.8	8.4	4.1	0.25
Finite Size Correction (FSC) (10^{-10} m^2 s^{-1})	2.5	2.5	1.0	0.03
Degree of dynamic dissociation (iconicity)	0.47	0.52	0.53	0.46
Conductivity (no FSC correction) (mS cm^{-1})	3.5	3.4	14.4	2.6
FSC corrected conductivity (mS cm^{-1})	3.9	3.8	15.8	2.8
Viscosity (mPa s)	0.48	0.48	1.4	35

Reference

(1) Ferrero, G. A.; Fuertes, A. B.; Sevilla, M., N-doped porous carbon capsules with tunable porosity for high-performance supercapacitors. *Journal of Materials Chemistry A* **2015,** *3* (6), 2914-2923.

(2) Büchel, G.; Unger, K. K.; Matsumoto, A.; Tsutsumi, K., A Novel Pathway for Synthesis of Submicrometer-Size Solid Core/Mesoporous Shell Silica Spheres. *Advanced Materials* **1998,** *10* (13), 1036-1038.

(3) Borodin, O., Polarizable Force Field Development and Molecular Dynamics Simulations of Ionic Liquids. *J. Phys. Chem. B* **2009,** *113* (33), 11463-11478.

(4) Yang, C.; Suo, L.; Borodin, O.; Wang, F.; Sun, W.; Gao, T.; Fan, X.; Hou, S.; Ma, Z.; Amine, K.; Xu, K.; Wang, C., Unique aqueous Li-ion/sulfur chemistry with high energy density and reversibility. *Proc Natl Acad Sci* **2017,** *114* (24), 6197-6202.

(5) Borodin, O.; Suo, L.; Gobet, M.; Ren, X.; Wang, F.; Faraone, A.; Peng, J.; Olguin, M.; Schroeder, M.; Ding, M. S.; Gobrogge, E.; von Wald Cresce, A.; Munoz, S.; Dura, J. A.; Greenbaum, S.; Wang, C.; Xu, K., Liquid Structure with Nano-Heterogeneity Promotes Cationic Transport in Concentrated Electrolytes. *ACS Nano* **2017,** *11* (10), 10462-10471.

(6) Borodin, O.; Giffin, G. A.; Moretti, A.; Haskins, J. B.; Lawson, J. W.; Henderson, W. A.; Passerini, S., Insights into the Structure and Transport of the Lithium, Sodium, Magnesium, and

Zinc Bis(trifluoromethansulfonyl)imide Salts in Ionic Liquids. *J. Phys. Chem. C* **2018,** *122* (35), 20108-20121.
(7) Andersen, A.; Rajput, N. N.; Han, K. S.; Pan, H.; Govind, N.; Persson, K. A.; Mueller, K. T.; Murugesan, V., Structure and Dynamics of Polysulfide Clusters in a Nonaqueous Solvent Mixture of 1,3-Dioxolane and 1,2-Dimethoxyethane. *Chem. Mater.* **2019,** *31* (7), 2308-2319.